Synthesis, characterisation and thermal behaviour of Cu based nano-multilayer

M. Czagány[1*], D. Varanasi[1], A. Sycheva[1,2], D. Janovszky[1,2], D. Koncz-Horváth[1], F. Kristaly[3], P. Baumli[1], G. Kaptay[1,2]

[1]Institute of Physical Metallurgy, Metal Forming and Nanotechnology, University of Miskolc, Miskolc-Egyetemvaros, 3515, Hungary
[2]MTA-ME Materials Science Research Group, Miskolc-Egyetemvaros, 3515, Hungary
[3]University of Miskolc, Institute of Mineralogy and Geology, Miskolc-Egyetemvaros, Hungary

*corresponding author, e-mail: czmatthews92@gmail.com

Abstract

In this paper, an example of a Cu based nano-multilayer (NML) as a potential material designed for joining applications is presented. For this purpose, Cu/AlN-Al_2O_3 NML was deposited by magnetron sputtering method on 42CrMo4 steel samples. The microstructure of the as-deposited and heat-treated multilayer was sudied by Scanning Electron Microscopy. Thermal behaviour of the multilayer was investigated by Differential Scanning Calorimetry, in-situ high temperature X-ray Diffraction and by performing heat treatment experiments. Starting from about 400 °C, extensive coarsening and migration of Cu nanocrystallites within the multilayer was observed via solid-state diffusion. Part of the initial Cu even formed micron-sized reservoirs within the NML. Due to increased temperature and to the different heat expansion coefficients of Cu and the AlN-Al_2O_3 diffusion barriers the latter cracked and Cu appeared on the top surface of the NML at 250 °C or even at a somewhat lower temperature. Below 900 °C the transport of Cu to the top surface of the NML probably took place as a solid state flow, leading to faceted copper micro-crystals on the top surface of NML. However, above 900 °C, the Cu micro-crystals found on the top of the NML have rounded shape. A possible explanation can be the pre-melting of nano-layered Cu due to its high specific surface area in the NML. Even if the Cu crystals appear on the top surface of NML via solid flow without pre-melting, these Cu crystals can provide joining at and above 250 °C (especially above 450 °C).

Keywords: nano-multilayer; copper; aluminium oxide; aluminium nitride; joining; melting point depression

1. Introduction

One of the difficulties of today's modern joining technology is the brazing/joining of heat-sensitive materials [1–6]. Metallic joints with high mechanical strength require high cohesion energy between the atoms of the metallic filler and of the materials to be joined, while the cohesion energy increases monotonously with the melting point of the filler [7, 8]. The most commonly used brazing materials are Cu (T_m: 1085 °C) [9], Ag (T_m: 962 °C) [10] and the eutectic Ag_{60}-Cu_{40} alloy (T_m: 779 °C) [11], which all require relatively high joining temperatures. In the case of brazing technology, one way to reduce the joining temperature is

to reduce the melting point of the braze filler itself, which is conventionally achieved by alloying (eg. with the addition of In, Zn, Sn, P, B). However, alloying may have undesirable disadvantages, such as toxicity (Cd), higher costs (In) and reduced mechanical or corrosion resistance [12, 13].

In recent years, a new approach, the application of nanotechnology has emerged in the practice of joining technology, just as in other fields of applied science and technologies. Reducing the dimensions of the phases below a certain size (<100 nm), their specific surface area is considerably increased, leading to melting point depression (MPD) and increased atomic mobility along internal interfaces (crystallite or phase boundaries) [14–18]. These properties cover the two most important parameters of the joining technology: thermodynamic (temperature) and the kinetic-transport (joining time) parameters.

Deposition of nano-multilayers (NML) on top of the parts/tools to be joined is one way to create nano-structured joining materials. There are various advanced coating technologies that can be applied effectively for this purpose, such as Physical Vapour Deposition (PVD) or Chemical Vapour Deposition (CVD). One type of these NML's is the group of reactive nanolayers [19–22], made up of periodically alternating layers of the brazing metal fillers (e.g. Al-Ti, Al-Ni, Al-Pd) with a few nanometer thickness. Thermal activation (heat or a single spark) triggers exothermic reactions, leading to the formation of intermetallic compounds inside the coatings, accompanied by the release of local heat. As a result, bond formation between the two components becomes feasible at lower temperatures, while the thickness of the resulting heat-affected zone can be reduced below 1 mm, reducing the risk to damage the heat-sensitive components.

Another approach is the development of nano-multilayered composite/hybrid joining materials, based on the concept emerged in the last decade [13, 23, 24]. This type of multilayer consists of a periodic repetition of a few nanometer thick metal (or alloy) layers and chemically inert barriers (usually oxides, nitrides, or refractory metals) [25, 26]. The purpose of the construction is to preserve the nano-thickness of the metal layers up to their melting point by separating them with the diffusion barriers. Thus, melting is assumed to occur at a lower temperature than that of the same metal of the macroscopic size. These multilayers can be applied as coatings of the materials to be joined, or as separate foils. The systems studied so far mainly include the metallic fillers of industrial importance: Ag, Cu, Ag-Cu and Al-Si based NML hybrid joining materials.

Lehmert et al. [27] studied the effect of heat treatment and brazeability of Cu/AlN nano-multilayers. The coating deposited by magnetron sputtering on Ti alloys consisted of 200 repetitions of 10-10 nm thick Cu and AlN layers. After heating at 750 °C, solifdified copper droplets were observed on the surface of the outer AlN layer. Based on their DSC measurements, the melting of copper in the range of 450-750 °C was assumed. As a result, a firm solid joint formed between the applied substrates at a temperature as low as 750 °C. On the basis of the experimental results, Kaptay et al. developed a thermodynamic model [16], in which the possibility of solid-state diffusion of Cu within the multilayer in addition to its melting was also considered.

A more extensively studied system is the Cu/W NML, where W serves as the diffusion barrier between the Cu layers. With the use of this multilayer, the formation of a joint similar to the mechanism of a diffusion bonding was observed at 750 °C [28]. The study of its thermal behaviour revealed the degradation of the multilayer structure, transforming into a spheroidized nanocomposite at 700 °C [29]. The migration of Cu to the surface of the multilayer and the feasibility of joint formation was attributed to the relaxation of the compression stresses accumulated in each layer mainly during the deposition process [30].

Nano-effects are more likely to be observed by reducing the layer thickness, however given the mechanism of film formation by PVD method, a minimum thickness value is also required, where a compact, laterally conttinuous coating formation is expected. In this respect, the 4 nm thickness was reported to be as a critical thickness [26]. As multilayers, consisting of 10-10 nm thick metal/ceramic layers were already reported and investigated in the literature, here we report on a multilayer with thinner, 5-5 nm individual layer thickness. Based on preliminary calculations, and experiments the AlN-Al_2O_3 ceramic layers are chemically inert to the Cu, and are not wetted by its melt, thus they can serve as separators and diffusion barriers for the Cu layers. The aim of the present study was to investigate in more detail the thermal behaviour of Cu/AlN-Al_2O_3 nano-multilayered hybrid composite.

2. Experimental

2.1 Deposition of Cu/AlN-Al_2O_3 nano-multilayer

Cu/AlN-Al_2O_3 nano-multilayer was deposited on top of 42CrMo4 (1.7225) steel plates (dimension of 10×7×4 mm, see chemical composition in Table 1) and α-Al_2O_3 wafers. Prior to deposition, the surface of the substrates was prepared by the following methods: mechanical grinding (grade of 500 and 800), polishing (down to 1 μm) followed by ultrasonic cleaning in

acetone (5 min). The Cu/AlN-Al_2O_3 NML was produced in a high-vacuum chamber (initial pressure $<5\times10^{-6}$ mbar) by magnetron sputtering method, using two confocally arranged unbalanced magnetrons, equipped with Cu (purity: 99.999%) and Al (purity: 99.999%) targets. First, a 15 nm thick AlN-Al_2O_3 sublayer was deposited on top of the subtstrates followed by 200 repetitions of periodically alternating Cu (5 nm) and AlN-Al_2O_3 (5 nm) nanolayers, reaching a total thickness of 2,000 nm. Consequently, the upmost layer was a 5 nm thick AlN-Al_2O_3 layer. The Cu layers served as metallic fillers, while the AlN-Al_2O_3 layers provided diffusion barriers for Cu. The related process parameters are listed in Table 2.

Table 1
Chemical composition of the 42CrMo4 steel substrate used in this study. First data line is the standard composition [31], second data line from our XRF measurements (Fe is the rest)

Chemical composition (wt%)						
C	**Si**	**Mn**	**Mo**	**P**	**S**	**Cr**
0.38-0.45	max 0.4	0.6-0.9	0.15-0.3	max. 0.025	max 0.035	0.9-1.2
XRF:	--	0.78	0.15	--	--	0.98

Table 2
Magnetron sputtering parameters to produce Cu/AlN-Al_2O_3 nano-multilayers

Process parameters	**Values for the corresponding layer**	
	Cu	**AlN-Al_2O_3**
Power source	DC	RF
Working pressure (mbar)	5×10^{-3}	7.5×10^{-3}
Ar flow (sccm)	90	90
N_2 and O_2 flow (sccm)	-	20
Current (mA)	110	-
Voltage (V)	620	-
Power (W)	68	150

2.2 Experimental setup and characterization techniques

The surface morphology and cross-section of the multilayer was analyzed by Hitachi S4800 Field Emission Scanning Electron Microscope (Japan) equipped with a Bruker AXS Energy-dispersive X-ray Spectrometer (EDS) system, and Helios G4 PFIB CXe Plasma Focused Ion Beam Scanning Electron Microscope (Czech Republic) equipped with EDAX Octane Elect EDS System with APEX™ Analysis Software. Higher magnification cross-sectional investigation was also carried out by FEI Tecnai G2 20 X-TWIN Transmission Electron Microscope (TEM) in the Laboratory of MTA-ME Materials Science Research Group. Cross-

sections for the measurement were prepared by mechanical method or with the use of Xe ion-beam milling and polishing function of the PFIB-SEM instrument, in order to obtain higher resolution.

XRD analysis of the as-deposited NML, and in-situ high temperature X-ray diffraction (HT-XRD) measurements were performed using a Bruker D8 Discover X-Ray Diffractometer (Germany) with Cu K-alpha radiation, 40 kV and 40 mA generator settings. Measurements were recorded with 0.007°(2Th)/24 seconds speed. In-situ high temperature experiments were carried out in Anton Paar HTK 1200N chamber attached to the XRD, in flowing Ar atmosphere. The chamber was automatically heated with a heating rate of 60 °C/min and the spectra were recorded at every 100 °C between 25-600 °C, then at every 50 °C between 600-1000 °C. The total time required to record one spectrum was 16.5 min, during which the sample was kept at a constant temperature. Crystalline phases were identified by Search/Match algorithm of the Bruker DiffracPlus EVA, using ICDD PDF2 database. The XRD measurement was performed in the 3DLab Fine Structure Analysis Laboratory of the University of Miskolc.

The thermal behaviour was further investigated by performing heat treatments of the Cu/AlN-Al_2O_3 NML coated 42CrMo4 seel samples in the range of 200…950 °C. For this purpose, a horizontal vacuum tube furnace (Sunplant Ltd., Hungary) equipped with CCD camera was used. After the insertion of the samples, the furnace was heated up to the desired temperature, and the samples were isothermally annealed in a range of ± 10 °C for 10 minutes with a working pressure of $7\pm2\times10^{-5}$ mbar. The samples were then cooled down to room temperature spontaneously inside the furnace. Wetting tests of Cu on the surface of AlN-Al_2O_3 ceramic layer were also preformed in the horizontal vacuum tube furnace, at a temperature of 1095±5 °C for 2 minutes, at a pressure of 2.5×10^{-4} mbar. The contact angle of the Cu droplet was measured with the use of the KSV software.

The thermal behaviour of the multilayer was investigated by means of Differential Scanning Calorimetry (DSC). In order to minimize any interfering sign of the substrate, α-Al_2O_3 substrates were used. Accordingly, smaller samples (appr. 3×4 mm) were cut out of the previously coated Al_2O_3 plate to fit in the crucible of the instrument. The measurement was performed in vacuum atmosphere of about 10^{-4} mbar with a heating rate of 10 °C/min. Before pumping, the instrument was filled with 99.999 % Ar several times to purge the system.

3. Results and discussion

3.1 As-deposited NML morphology and microstructure

Microstructural images of the as-deposited Cu/AlN-Al_2O_3 NML are shown in Figure 1. The surface is relatively uniform without cavities. However, the traces of the polishing process preceding the NML deposition are slightly tracked by the multilayer (Fig. 1a). The grain-like morphology of the surface is characteristic of PVD coatings, but does not indicate a real grain/crystallite structure, rather it is a consequence of the increasing waviness of each deposited layer, observed similarly in the case of metal based [32] and ceramic based nano-multilayers [33, 34]. High-resolution cross-sectional images of the individual layers are shown in Figure 1b. The lighter layers indicate Cu while the darker layers indicate AlN-Al_2O_3. Fig. 1c shows a higher magnification TEM image of the cross-section of the multilayer. In this image, the darker layers relate to Cu and the lighter ones are the ceramics. The laterally continuous structure of the individual layers is well resolved. The actual thickness of the Cu layers is measured about 6.7 nm, the same for the AlN-Al_2O_3 barrier layers is found about 4.8 nm, while that for the first AlN-Al_2O_3 layer is found about 15.5 nm. The measured total thickness of the multilayer is 2,250 nm. Some waviness of the layers is observed, which might be attributed to the combined effect of the unevenness of the substrate surface as seen in Fig.1b, and to the 3D growth mode of the layer during the PVD process [29, 35]. The waviness of the layers can be characterized by the vertical peak-to-valley distance, which is found in the interval of 6.8 …12.27 nm for Cu and 4.9 … 10.6 nm for the AlN-Al_2O_3 layers. The elemental composition of the multilayer, obtained on the surface of the multilayer is listed in Table 3. The presence of Fe originates from the steel substrate, which suggests an interaction depth of the electron beam slightly larger than 2250 nm. It is worth noting that with the use of EDS, the quantitative analysis of O and N is not sufficiently accurate, thus no further conclusions can be drawn from it.

Table 3
EDS composition of Cu/AlN-Al_2O_3 NML deposited on 42CrMo4 steel substrate

Element		Cu	Al	O	N	Fe
Composition	w%	72.2	10.7	6.6	6.4	4.1
	at%	45.9	16.1	16.7	18.5	2.9

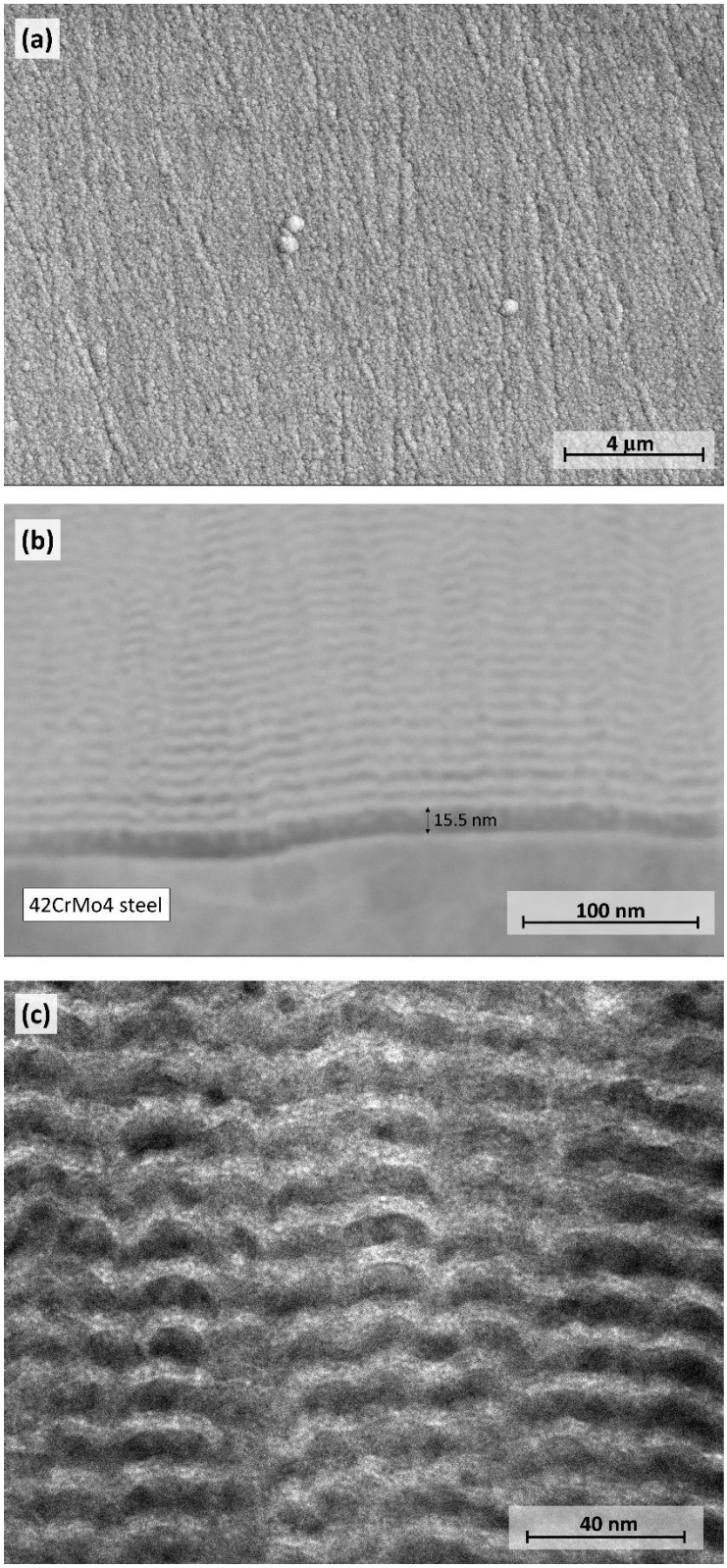

Fig. 1 PFIB-SEM image of the top surface of Cu/AlN-Al_2O_3 NML deposited on 42CrMo4 steel (a), cross-sectional PFIB-SEM image of the multilayer (b), Higher magnification TEM image of the cross-section of the multilayer

The XRD diffractogram of the as-deposited Cu/AlN-Al_2O_3 NML is shown in Figure 2. The reflections of α-Fe (ferrite) originate from the 42CrMo4 steel substrate. In the range of $2\Theta = 41$

… 44.5° superimposed reflections are identified, originated from the multilayer: Cu (111), AlN (200) and from the surface of the steel: FeO (200) and Fe_3N ($\bar{1}\bar{1}1$). In addition to superimposition, the presence of Cu is indicated by a broader peak at $2\Theta = 43.2°$, which is attributed to its nanocrystalline structure and may also reflect to residual stresses developed during the deposition process [36]. Lower intensity peaks of AlN (111) and (200), as well as α-Al_2O_3 (104) and (024) are indicative of the complex phase-structure of the barrier layers. The presence of Fe_3N and FeO are the reaction products between the Fe surface atoms of the steel substrate and the plasma-activated N and O, during the deposition of the first AlN-Al_2O_3 sublayer. However, it is worth noting that superlattice reflections, originated from the periodic layered structure might also contribute in the ranges between $2\Theta = 33 … 38°$ and $2\Theta = 41 … 45°$ as observed for other nano-layered systems [29, 37, 38].

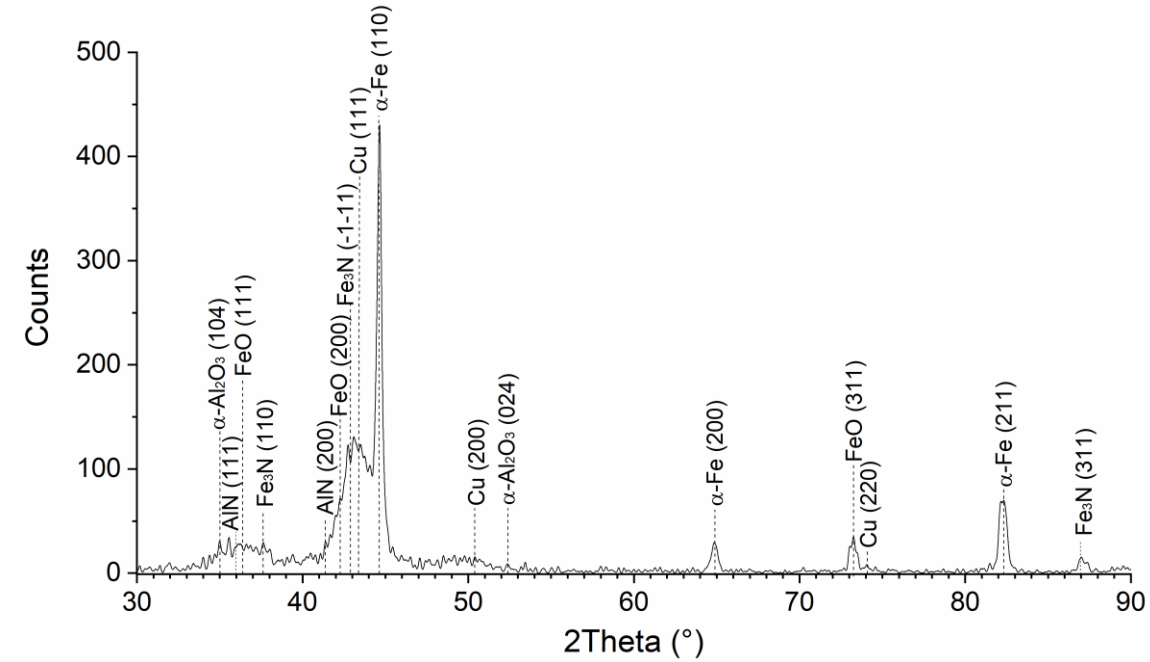

Fig. 2 XRD diffractogram of as-deposited Cu/AlN-Al_2O_3 NML on 42CrMo4 steel substrate, measured at room temperature (25 °C)

3.2 Phase evolution during heat treatment

The evolution of the phase-structure was monitored and investigated by high-temperature X-ray diffraction (HT-XRD) measurement. Changes of the superimposed reflexions in the range of 41…44.5° can be seen even at lower temperatures (200-300 °C), reflecting some structural transformation within the multilayer (Fig. 3) The Cu (111) reflection became more pronounced at and above the temperature of 400 °C, which is characteristic of microscale grain structure,

indicating coarsening of Cu nanocrystallites. However, the broadened character of the curve in the vicinity of the evolving Cu reflection is still observed, indicating that some part of Cu remains in nano-confinement.

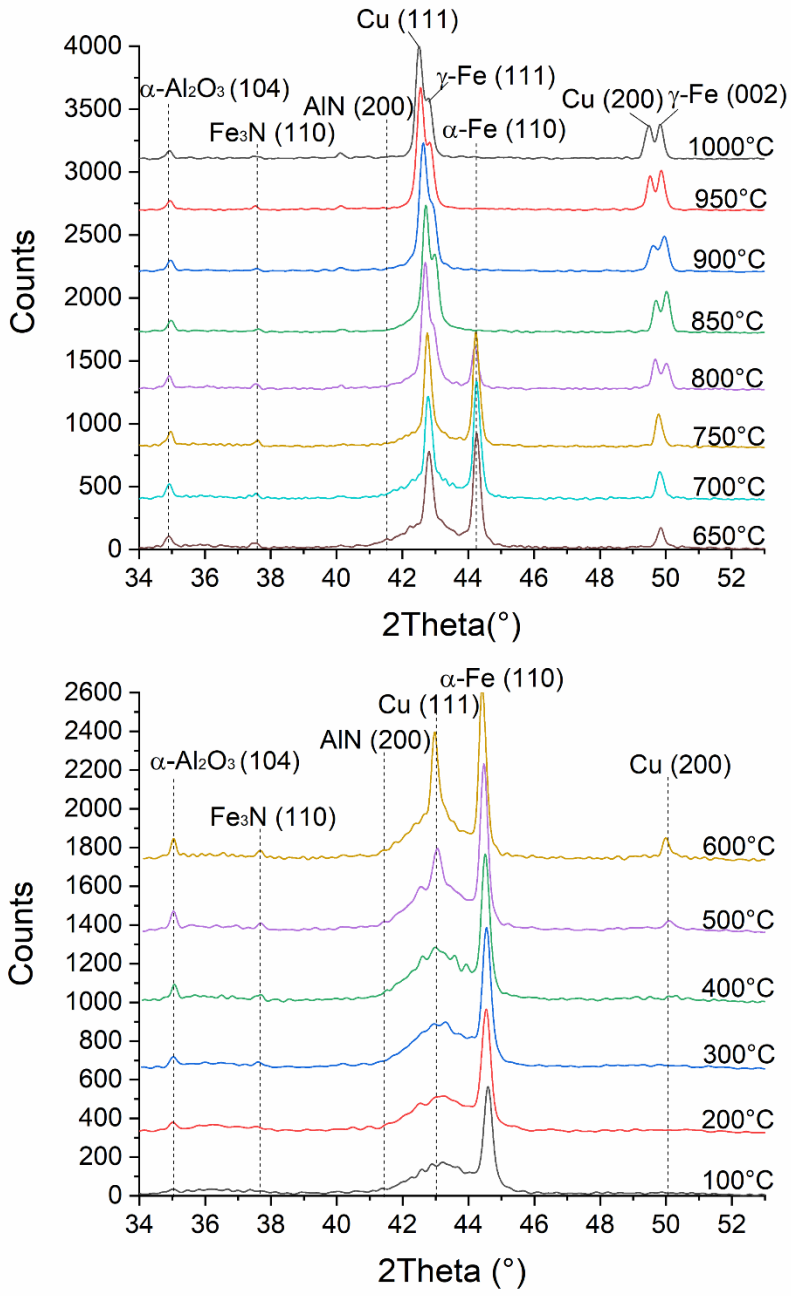

Fig. 3 HT-XRD spectra of Cu/AlN-Al_2O_3 NML deposited on 42CrMo4 steel substrate, in the temperature interval of 100-600 °C (a) and 650-1000 °C (b)

The evolution of α-Al_2O_3 (104) reflection into a more characteristic one with increasing temperature is another process being detected. At the same time, the peak of AlN (200) declines with temperature, indicating that AlN is continuously converted into Al_2O_3 with increasing temperature, which is a thermodynamically favoured process in the presence of excess oxygen

/ nitrogen (see Fig.4). The AlN→Al_2O_3 conversion leads to the release of nitrogen and to the additional formation of the Fe-nitride phase, confirmed by the intensity growth of the Fe_3N (110) peak in Fig.4 (see also Fig.4). Heating from 600 to 1000 °C results in further decrease in the amout of AlN (Fig.4b), which eventually disappears at about 800 °C. The appearence of austenite reflections at about 800 °C indicates the allotropic transformation of the steel substrate. The broad peak in the vicinity of the Cu reflection (2Θ = 43.2°) is continuously suppressed, suggesting a decrease in the proportion of nano-thin Cu layers, that remained within the multilayer structure.

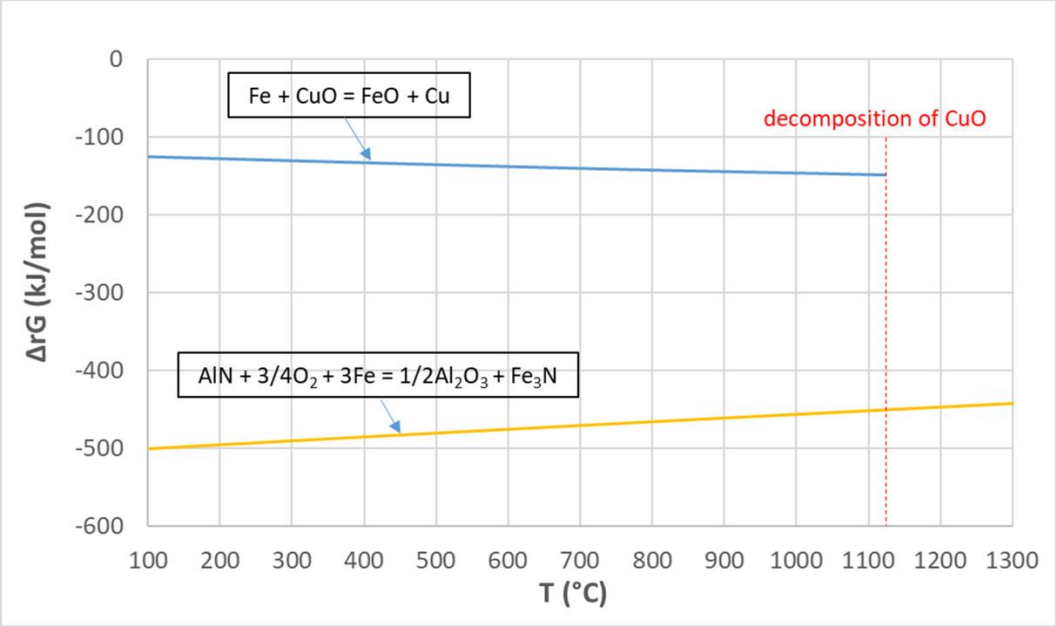

Fig. 4 Calculated standard Gibbs energy changes accompanying some reactions [39] (note that the standard Gibbs energy of formation of iron nitride is taken as zero for simplicity – see also [40]). The vertical dotted line indicates the temperature of the decomposition of CuO

3.3 Wettability of Cu/AlN-Al_2O_3 system

The wetting properties of Cu/AlN-Al_2O_3 system was also investigated, as an important feature to understand the behaviour of the nano-multilayered system. For this purpose, a 340 nm thick AlN-Al_2O_3 ceramic monolayer was deposited on C45 (1.0503) steel plate by magnetron sputtering method. Then, a small piece of Cu (purity of 99.76%) was placed on top of the ceramic layer, and the assembly was inserted in the vacuum tube furnace. Images of the Cu can be seen in Fig. 5 before (Fig. 5a) and rigth after (Fig. 5b) melting. The obtained contact angle of Cu is θ=123 ± 5°, refering to poor wetting (see Fig. 5b). This result is in close agreement with the literature data [41, 42]. The poor wetting of the Cu/AlN-Al_2O_3 system allows that the melted Cu would not prefer remaining confined between the ceramic layers, rather would prefer

to flow/migrate out of the layers to the top surface of the multilayer, which is a prerequisite of succesful joining.

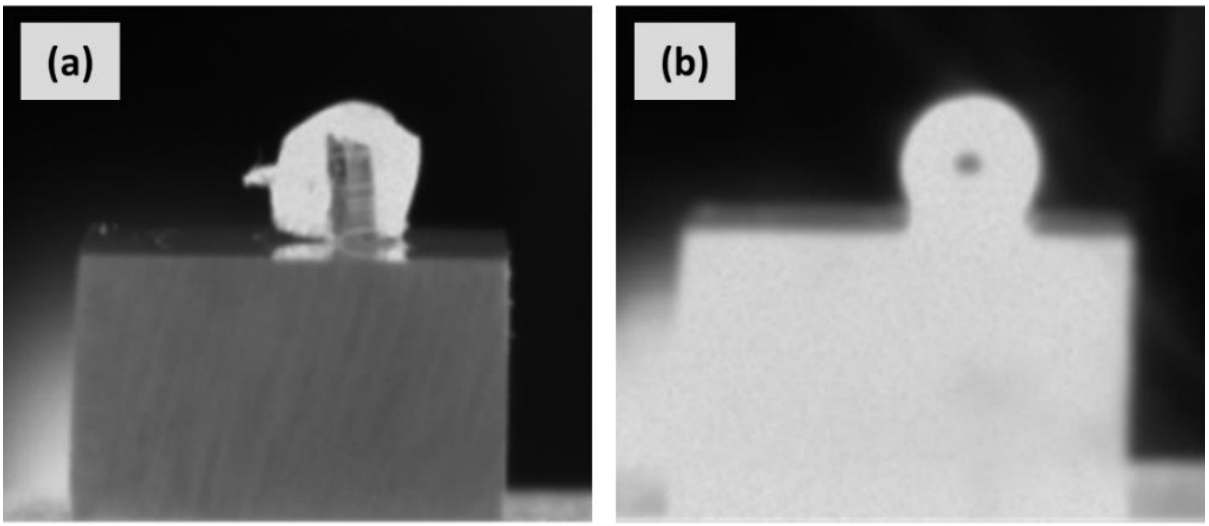

Fig. 5 A piece of Cu on top of AlN-Al_2O_3 coated C45 steel before (a) and right after (b) melting

3.4 Microstructural evolution during heat treatment

In order to get a deeper understanding of the thermal behaviour of the multilayer, heat treatment experiments were performed at temperatures of 200, 250, 350, 450, 550, 650, 750, 850 and 950 °C. SEM images of the surface of the multilayer, isothermally kept at 450 °C are shown in Fig. 6. Different line-shaped structures as well as separate protrusions can be observed on the surface. The linearly arranged formations are identified as Cu crystals (Fig. 7). These Cu crystals were found to appear on the top surface on the multilayer from the temperature of 250 °C. Although a similar phenomenon was previously reported by Lehmert et al. [27] at 750 °C, let us mention that in our case the same is observed at much lower temperatures. It is worth noting, that the appearence of Cu on the top surface of the multilayer is a criterion considering joining applications. Higher magnification (see Fig. 6b) reveals that these linear structures are made up of irregularly shaped, but faceted Cu crystals with their sizes above a micrometer. Thus, the original Cu nano-layers appeared at least partly on the top surface of the NML and are transformed into micron sized crystals. The linear arrangement of the Cu crystals is remarkable, and can be explained by a surface crack (see Fig. 6b), which is partially filled by the Cu crystals. In other words, the Cu micro-crystals appeared on the top surface through the crack in the ceramic layers.

These observations are explained here by the large difference between the linear expansion coefficient of Cu ($\alpha_{Cu}=16.5\times10^{-6}$ 1/K) [43] and that of the ceramic barrier layers ($\alpha_{Al2O3}=8.1\times10^{-}$

^{6} 1/K [44] and $\alpha_{AlN}=4.8\times10^{-6}$ 1/K [45]). During heating, this heat expansion mismatch lead to a continuosly increasing inner pressure within the NML, which eventually resulted in the cracking of the ceramic barrier layers, which allowed the outflow of copper to the surface. Moreover, as these cracks represent a lower energy state, Cu is preferentially located along them on the top of the NML. This phenomenon is similar to the hypothesis made in connection with the thermally annealed Cu/W nano-multilayers [29], although contrary to our present paper no visible cracks were detected in that paper (see also [46]).

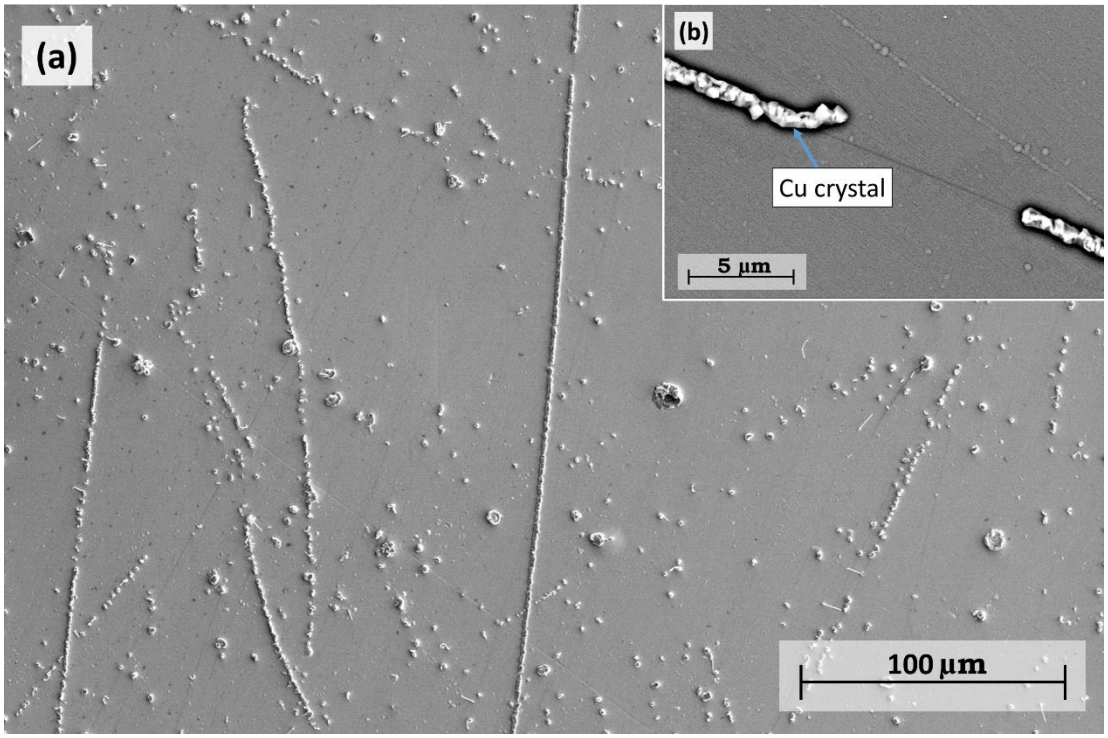

Fig. 6 PFIB-SEM image of the top surface of Cu/AlN-Al_2O_3 NML deposited on 42CrMo4 steel substrate, heat-treated at 450 °C (a), higher magnification of the linearly-arranged Cu on the surface (b)

The elemental map (Fig. 7) and the line-scan across the crystals (Fig. 8) confirm that the crystals observed at the top surface of NML are indeed pure Cu crystals and are only slightly oxidized on their surface. This confirms that while Cu is within the NML in the form of 6.4 nm thin nano-layers, it is safe from oxidation. However, when it is flown out to the top of the NML through the cracks, its surface is oxidized below 900 °C, in accordance with the phase diagram of Fig.9 (see the cross section of the „Cu_2O/Cu(s)" line with the „p2" line). Similarly, Cu(O) was observed on the surface of Ag_{60}-Cu_{40}/AlN nano-multilayer, heat-treated in air atmosphere [26]. As follows from Fig. 9, the vacuum with residual pressure of $7 \pm 2 \times 10^{-5}$ mbar used in our experiments is sufficient to ensure oxide-free Cu only above 900 °C. On the other hand,

after the Cu-oxide layer with thickness of about 10 nm is formed on the top of micron sized Cu crystals, further oxidation is slowed down as it is limited by solid state diffusion.

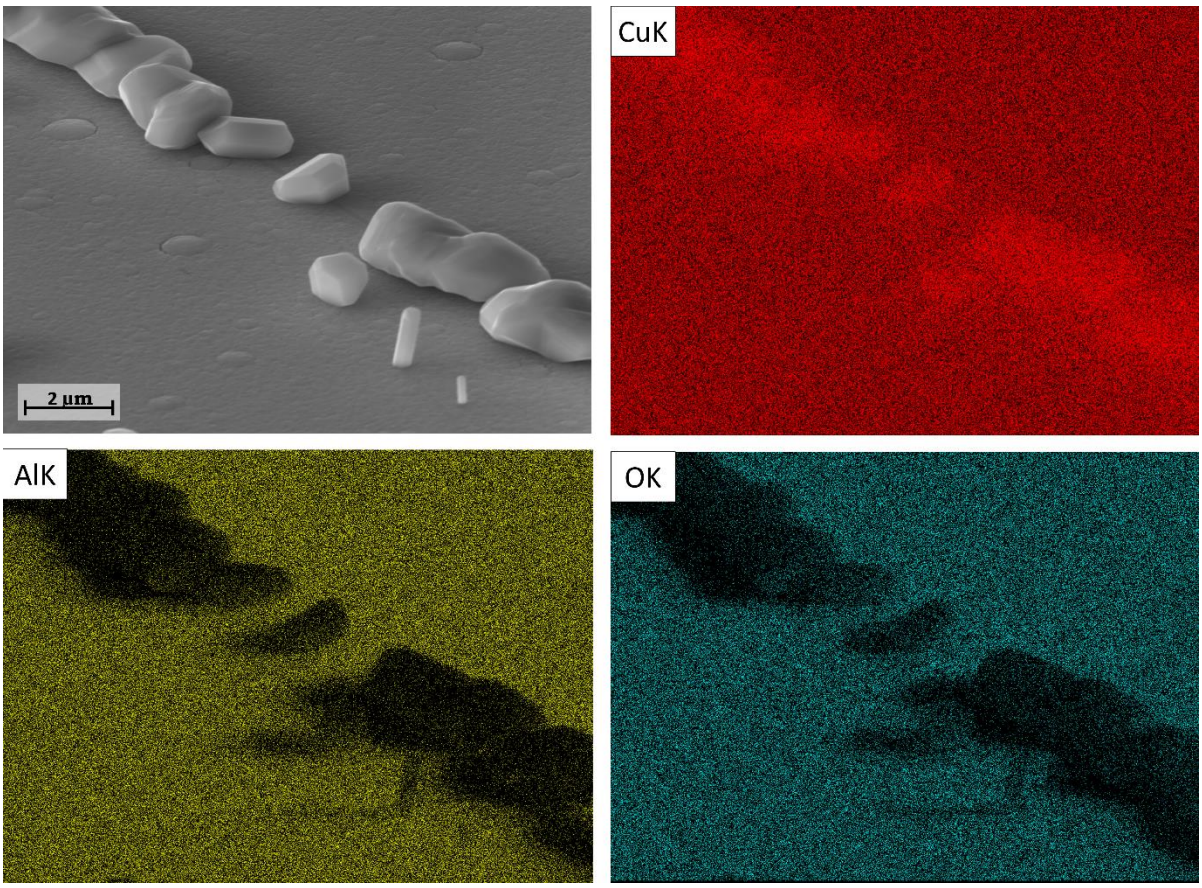

Fig. 7 Elemental map (O, Al, Cu) of the Cu crystals observed on the surface of Cu/AlN-Al_2O_3 NML, heat-treated at 550 °C.

It is worth to mention that the Cu-crystals on top of NML seem natural metallic in light microscope, confirming the oxide layer is not too thick on them. Although oxide films might change the visible color of metals [47], but only above a critical thickness [48]. Using Eq.(10a) of [48] the smallest thickness of the copper oxide layer of 37 nm is found that ensures the minimum of 400 nm wavelength of destructive interference if the refractive index of the CuO / Cu_2O taken as 2.7 ± 0.1 (see p. 236 of [44]), where 400 nm is the lowest wavelength of light visible by humans. This means the thickness of the oxide layer on the micron-sized Cu-crystals is surely below 37 nm, which is less than 2 % of the total size of the Cu-crystals, explaining why the presence of oxygen on Cu crystals seems negligible in Fig-s 7-8. From this maximum oxide thickness of 37 nm and from the molar volumes of Cu (7.09 cm^3/mol [43]), CuO (12.4 cm^3/mol [44]) and Cu_2O (23.9 cm^3/mol [44]) one can estimate the initial thickness of the Cu layer that is oxidized being below 11 nm. As for joining application metallic Cu is required,

these findings suggest that the degree of Cu oxidation can be considered negligible in the used vacuum environment.

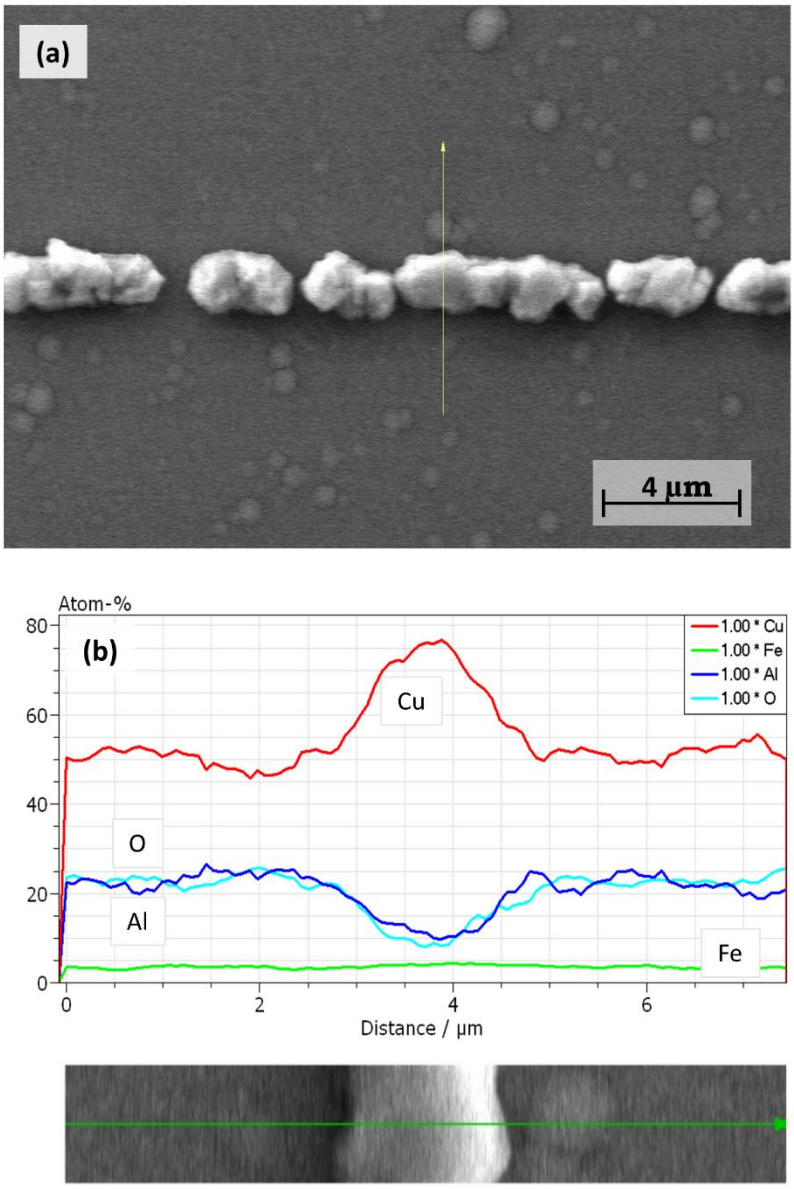

Fig. 8 Cu crystals at the top of the NML after 450 °C of heat treatment (a) and the line-scan across one of them (b) (some Fe is visible below the NML from the steel substrate)

In addition to Cu-crystals aligned along a line due to the long crack below them, there are also separate surface protrusions visible in Fig. 10a, where a locally protruded part of the nano-multilayer can be seen surrounded by Cu. For further investigation, a slope cut was applied to obtain the cross-section of the multilayer (see Fig. 10b). Cu enrichment accumulated within the multilayer was found in a micron-sized reservoir with about 1.0 µm height and about 6.5 µm length. As the Cu reservoir is formed, the multilayer above it is locally protruded from its initial surface (Fig. 10a). The driving force for this process is surface energy reduction due to

coarsening of initially nano-thin Cu layers [18] and the non-wetting property of Cu on the surface of AlN-Al_2O_3 [49], as our contact angle measurement confirmed it further (see Fig. 5b). As follows from Fig. 10b, a moment was captured by cooling the sample when the accumulated Cu in the reservoir only partly flew out to the top surface of the multilayer, via a channel formed within the Cu-depleted ceramic layers, leaving a void behind. Let us mention that to form a micron-sized Cu-reservoir in addition to the in-plane diffusion of Cu within one nano-layer also copper diffusion from a number of Cu-layers through the defects in the ceramic layers should have been taking place.

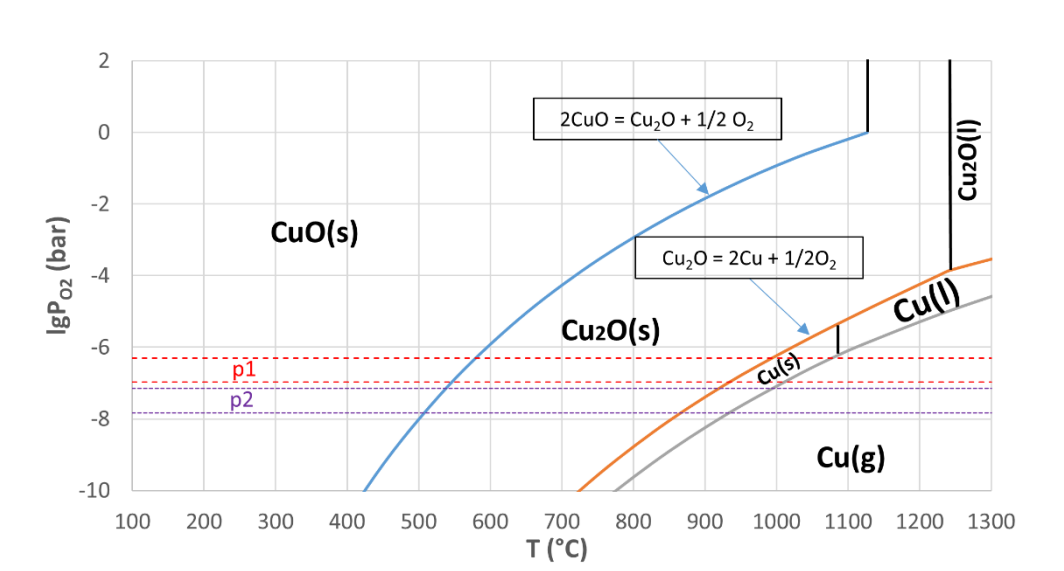

Fig. 9 Calculated phase diagram of the copper - oxygen system (thermodynamic data by [39] were used), p1: the pressure interval of the DSC measurement, p2: the pressure interval of the heat treatment experiments, as the oxygen content of the air is 21%, the experimental pressure conditions are expressed in intervals (0.21*p … p, where p is the remaining pressure)

SEM images of the top surface of Cu/AlN-Al_2O_3 NML heat-treated at 550 °C, 650 °C, 750°C, 850°C and 950°C are shown in Fig. 11. At 550°C and 650 °C, typically faceted Cu crystal shapes were observed, with an increased size of above 1 µm (Fig. 11a and b). In addition, a very interesting process is shown in Fig. 11b, the formation of Cu whiskers from the faceted Cu crystals. The diameter of these whiskers is between 115-600 nm, while their length was found between a few hundred nm to 45-50 µm. These whiskers were observed on the surface of the NML from the temperature of 350 °C. The largest amount of these whiskers were found at 650 °C, while with increasing temperature, the number of these whiskers decreased. The formation of whiskers is commonly observed in the case of tin (Sn), usually in contact with Cu [50]. The main driving force behind them is the generated mechanical stress as a result of intermetallic layer formation [51] or outer mechanical pressure [52]. The formation of the whiskers results in the relaxation of the accumulated stresses. Beside Sn, other metallic

whiskers were observed in the case of Al [53] or Ag [54]. In the case of Cu, Cu_2O whisker formation was reported by B. Horváth et al. [55]. In their case, Sn-Cu alloy coated Cu substrates were subjected to corrosive high-temperature and humidity (105 °C, 100% RH) which caused the formation and growth of Cu_2O whiskers from the Sn-Cu coating.

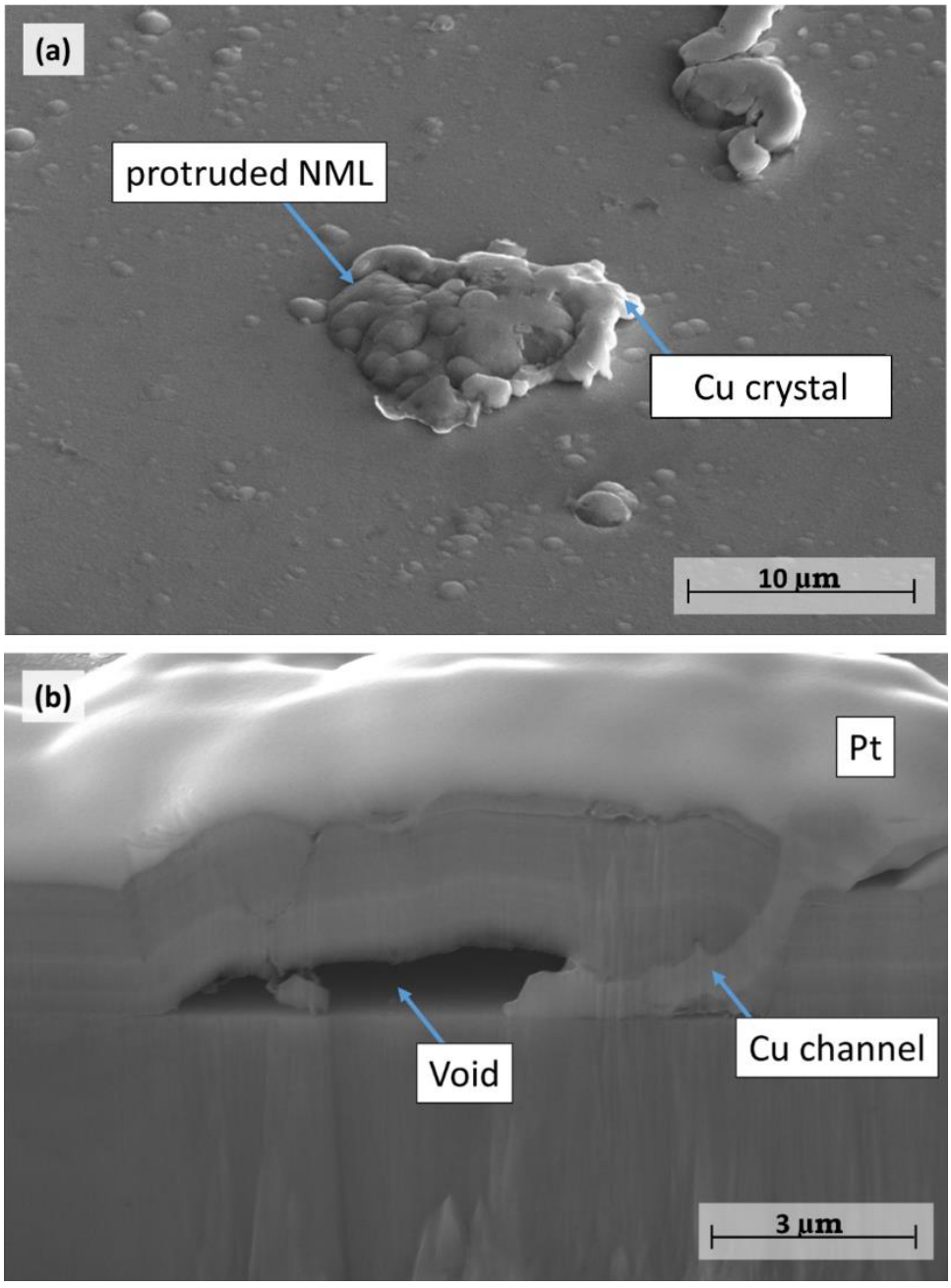

Fig. 10 PFIB-SEM image of the surface of Cu/AlN-Al_2O_3 NML, heat-treated at 450 °C showing a surface protrusion surrounded by Cu (a), cross-section of the same across the protrusion, cut by Xe ion-milling process (b)

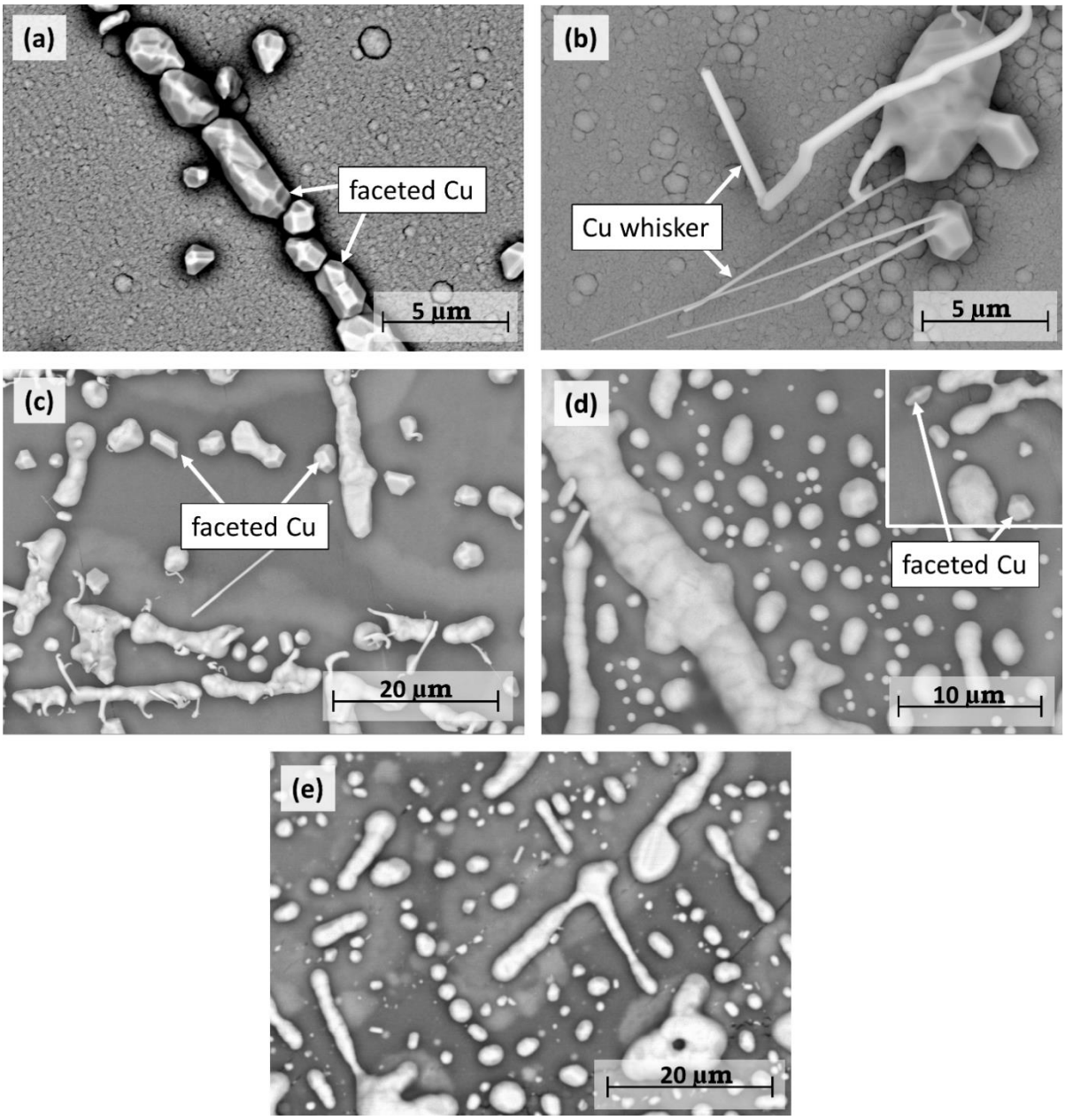

Fig. 11 SEM images of the surface of Cu/AlN-Al_2O_3 NML deposited on 42CrMo4 steel, faceted Cu crystals at 550 °C (a) formation of Cu whiskers from the faceted crystals at 650 °C (b), Cu crystals at 750 °C (c), 850 °C (d) and 950 °C (e). Note that crystals are faceted in (a-c) and becoming rounded in (d,e)

With increasing temperature the amount of the Cu crystals on the top of NML increased. Moreover, the faceted crystals found between 250-750 °C starts to turn into rounded (droplet shaped) when temperature becomes as high as 850 °C (Fig. 11d). Thus, it would follow that Cu was probably melted in the T-interval between 750 …850 ºC. However, Cu micro-crystals can not melt at this low temperature, as pre-melting could take place only within the NML structure. Let us mention that the faceted – rounded „transformation" can also take place via solid state diffusion with its driving force being the reduction of the specific surface area of the crystal [18].

Cross-section of a Cu reservoir situated within the nano-multilayer, previously heat-treated at 650 °C is shown in Fig. 12a. A crack of the Cu-depleted AlN-Al_2O_3 layers is also observed below a surface Cu crystal (Fig. 12b), allowing Cu to get to the top surface. The width of one of these cracks is 24.6 nm. Let us note that not all copper appears on the top surface of the multilayer. As it follows from Figs 12c-d, some copper remains within the NML in the form of accumulations even after it was heat treated at 950 °C. The size of these accumulations are considerably larger than that of the reservoir sizes observed at lower temperatures. It is reasonably considered, that with increasing temperature the size of the Cu reservoirs grew steadily. Moreover, the separate small reservoirs that came into contact eventually merged, decreasing further their specific surface area. The previously observed voids (at 450 °C) remained after the Cu outflow are no longer visible at higher temperatures, referring to the restoration of the original positions of the nano-multilayer.

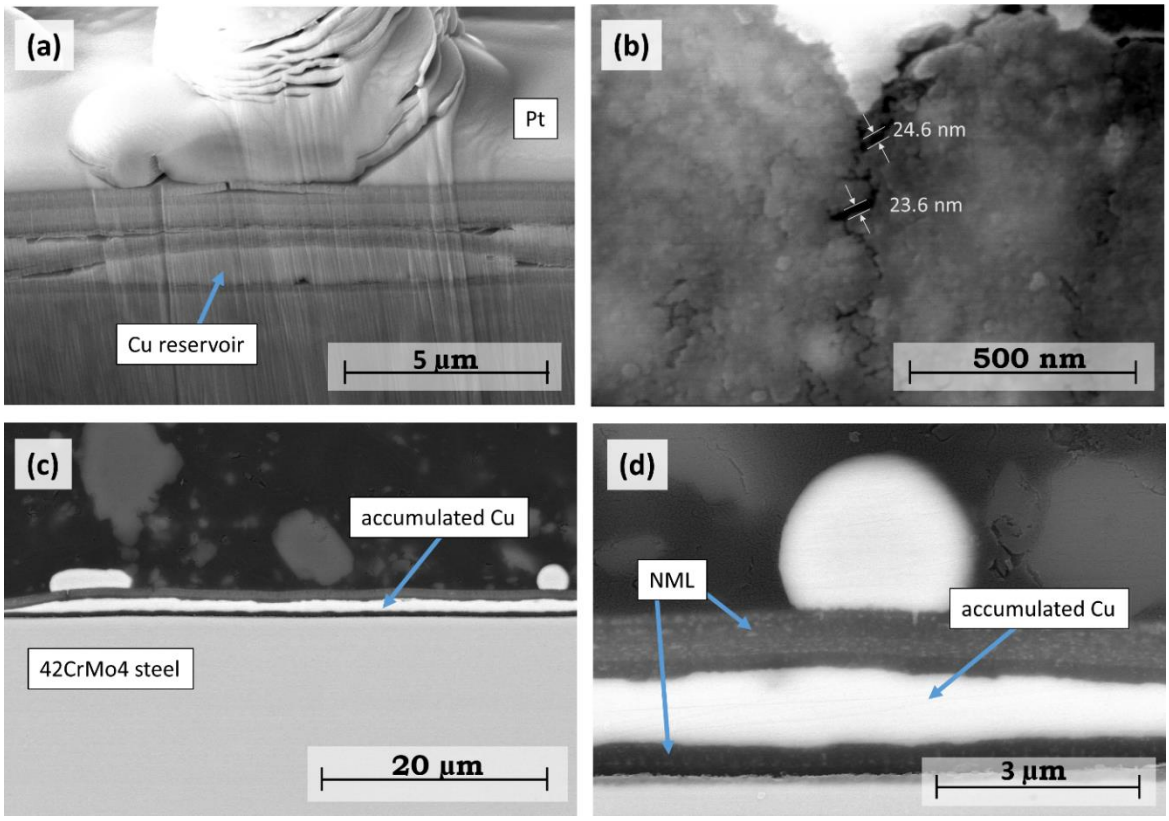

Fig. 12 SEM images of Cu/AlN-Al_2O_3 NML deposited on 42CrMo4 steel. Cu reservoir within the NML after heat treatment at 650 °C (a), a crack observed below a Cu crystal after heat treatment at 850 °C (b), accumulated copper within the NML sturcture after heat treatment at 950 °C (c-d)

Furthermore, some part of Cu remained in nano-confinement as follows from Fig.13, showing the remaining part of copper in between the ceramic layers as function of temperature. During the measurement, the diameter of the electron beam was approx. 1 µm, and the concentration of Cu was measured at a reasonable distance from the Cu reservoirs. It is shown that about 25

% of Cu remained within the NML even after it was heat treated at 950 °C. However reaching the temperature of 1100 °C (above the bulk melting point of Cu) it was found that no Cu remained in between the ceramic layers of the NML.

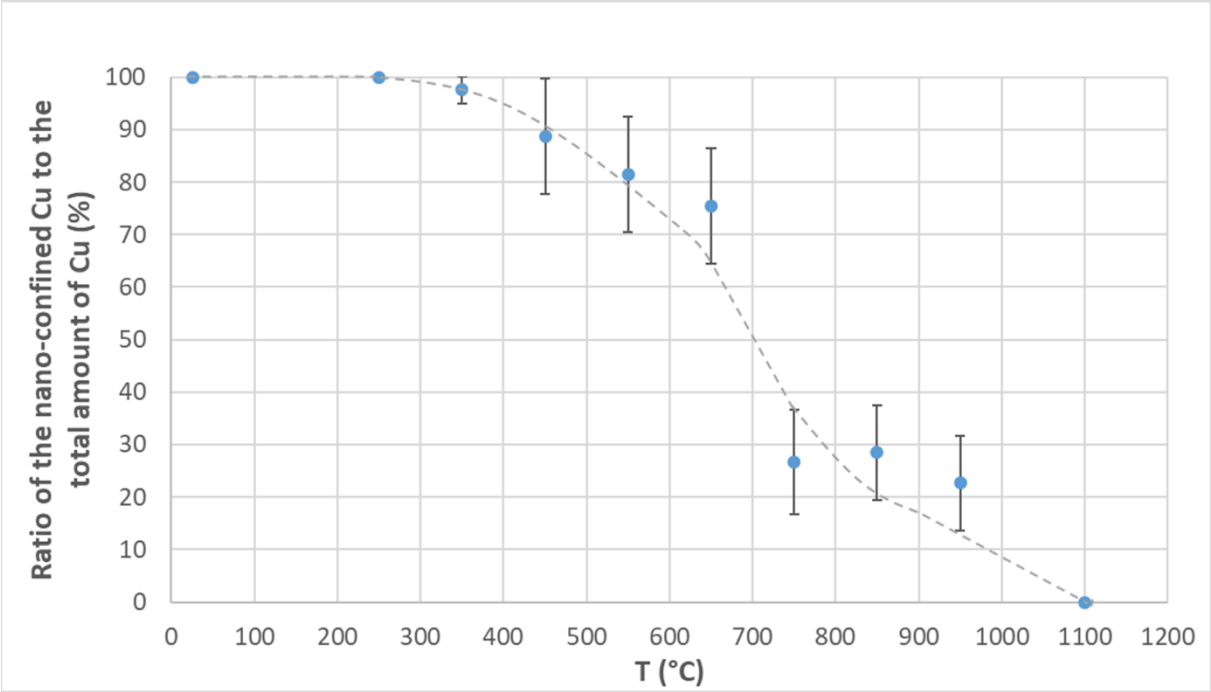

Fig. 13 The amount of Cu remained between the AlN-Al_2O_3 nano-layers as a function of the heat treatment temperature, obtained by EDS measurement

3.5. Differential scanning calorimetry of the NML

Figure 14 shows the DSC graph obtained from the original Cu/AlN-Al_2O_3 NML deposited on alumina substrate. In Fig.14 first a rather broad, low-intensity exothermic peak appears in the temperature range of 400 … 800 °C, followed by a second, also broad, but high-intensity endothermic peak in the temperature range of 954 … 1250 °C. Fig. 14 will be used to summarize (and confirm additionally) the processes discussed above.

The onset temperature of the exothermic process (around 400 °C, see Fig. 14) coincides with the beginning of the extensive grain coarsening of Cu nanocrystallites, observed during the XRD measurement (see Fig. 3a). Let us mention that a similar exothermic peak was explained by Ohnuma et al. [56] by the „clustering" of Cu in their FINEMET type amorphous alloy. Let us check if clustering – coarsening of Cu nano-layers can indeed explain the exothermic process accompanied by -5.6 J/g heat relase, as follows from Fig. 14. As the total mass of the measured sample (together with alumina substrate) was 0.153 g, the total measured exothermic heat effect in Fig. 14 was re-calculated to -0.857 J. Now let us estimate how much heat can be released if all Cu in the NML is coarsened more than by 2 orders in magnitude, when its final specific

surface area becomes negligible compared to its original specific surface area [18]. For that, first let us evaluate the initial surface area of Cu. The total surface area of one side of the small samples used for the measurement was around 132 mm^2. Multiplying this value by the number of Cu nanolayers (200), by 2 (for the two sides of each Cu nano-layer), by 2 (for the wavy nature of the NML shown in Fig.1b) and by 0.75 (for the ratio of coarsened Cu after Fig.13) the total initial interfacial area of Cu nanolayers is found as 0.0792 m^2. Now, let us estimate the enthalpy part of the surface energy of solid Cu (= the maximum possible specific heat loss due to coarsening), similarly as it was done by Yakymovych et al [57], extrapolating the surface energy of the metal to T = 0 K, which equals about 2.50 J/m^2 (see Eq.10b in [8] and data from [39] and [58]). Multiplying this surface energy by the above found initial interface area, the maximum exothermic heat of -0.198 J follows. As compared to the above -0.857 J one can conclude that coarsening of Cu in our experiments can lead to maximum of about 23 % of the measured heat release.

Therefore, some additional explanation is needed to rationalize the exothermic effect observed in Fig.14. As was already discussed in relation with Fig.8 the surface of the Cu crystals that appeared on the top of the NML at 450 $^{\circ}C$ is at least partly oxidized. The heat of oxidation in the temperature range of the exothermic peak in Fig.14 is about -127 ± 10 kJ/mol-Cu for CuO and -61 ± 3 kJ/mol-Cu for Cu_2O [39]. The total amount of Cu on the top of the NML is the above mentioned 132 mm^2 multiplied by 6.4 nm (the average thickness of each Cu nano-layer), by 200 (the number of Cu nano-layers), by 0.75 (from Fig.14) and divided by 7.09 cm^3/mol (the molar volume of Cu) = 1.79×10^{-5} mol. Multiplying it by the above given possible range of -137 … -58 kJ/mol-Cu the resulting heat effect is -1.04 … -2.45 J. The missing exothermic heat after coarsening (-0.857 + 0.198 = -0.659 J) is 27 … 63 % of the oxidation heat. The average crystal size of Cu from Fig. 6b is about 1 micron and it is approximately cubic in shape. The 27 … 63 % of the amount of matter of a 1 micron cubic crystal takes its outer 10 … 28 %, which corresponds to about 100 … 280 nm thick surface oxide layer. However, this contradicts the above observation that the thickness of the surface oxide layer is surely below 11 nm. So, the oxidation heat of copper micro-crystals is at most -0.1 J. This leaves -0.857 + 0.198 + 0.1 = -0.559 J of additional exothermic heat. Therefore, coarsening and surface oxidation of Cu taken together are still not sufficient to explain the exothermic effect observed in Fig. 14. An additonal exothermic effect is connected with the oxidation of AlN to Al_2O_3 as proven above in Fig. 3. This is also confirmed by Fig. 15 proving that under our experimental conditions (temperature and oxygen/nitrogen partial pressure) the chemical reaction $2AlN + 1.5O_2 = Al_2O_3 + N_2$ is

shifted to the right. The standard heat of this reaction is about -507 ± 3 kJ/mol-AlN in the temperature range of the exothermic peak in Fig.14. Suppose that the ceramic nano-layers are made fully of AlN. Then the initial maximum total amount of matter of AlN in the NML is calculated as 132 mm^2 (surface area of NML from one side) multiplied by 200 (number of nano-layers) and by 4.2 nm (thickness of one cderamic nano-layer) divided by 12.8 cm^3/mol (the molar volume of AlN [59]) = 8.66 10^{-6} mol. If this amount of AlN is multiplied by the above given heat of reaction (-507 kJ/mol), the maximum exothermic effect obtained from the oxidation of AlN is -4.39 kJ. Compared to the missing -0.524 J (see above) one can conclude that the oxidation of only 12 % of the maximum initial amount of AlN is sufficient to reproduce the exothermic heat found in Fig.14.

Summarizing, the broad exothermic heat found in Fig.14 (-0.857 J) is made of about -0.198 J (23 %) of coarsening heat, -0.10 J (12 %) of surface oxidation of the micron sized Cu crystals and -0.557 J (65 %) of oxidation of AlN. These 3 processes explains why the broad exothermic peak in Fig.14 contains 3 sub-peaks.

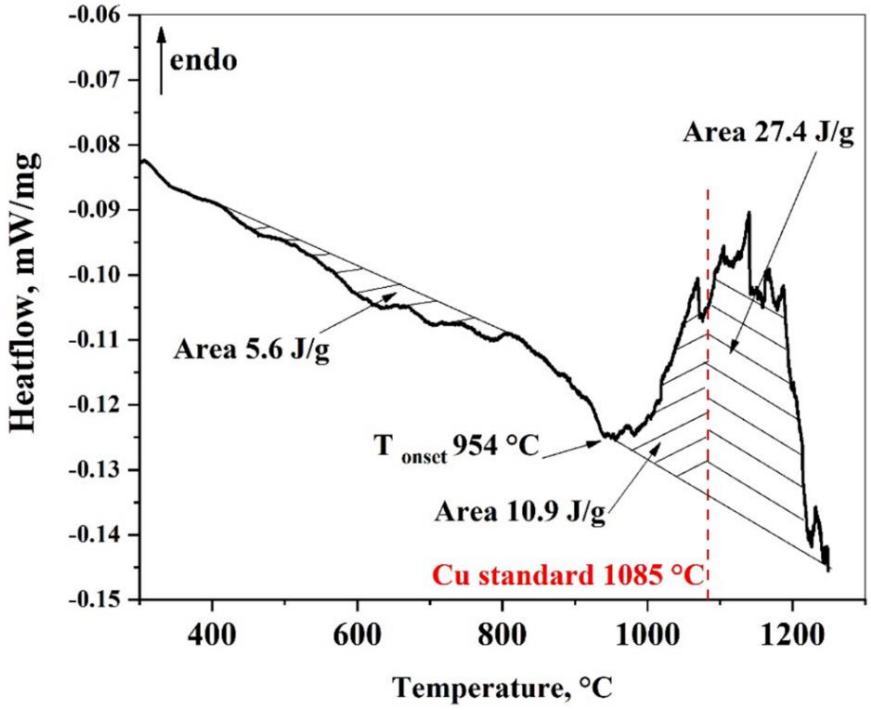

Fig. 14 DSC graph of Cu/AlN-Al_2O_3 NML deposited on α-Al_2O_3 substrate, heating rate: 10 °C/min (vertical dotted line: macroscopic melting point of Cu)

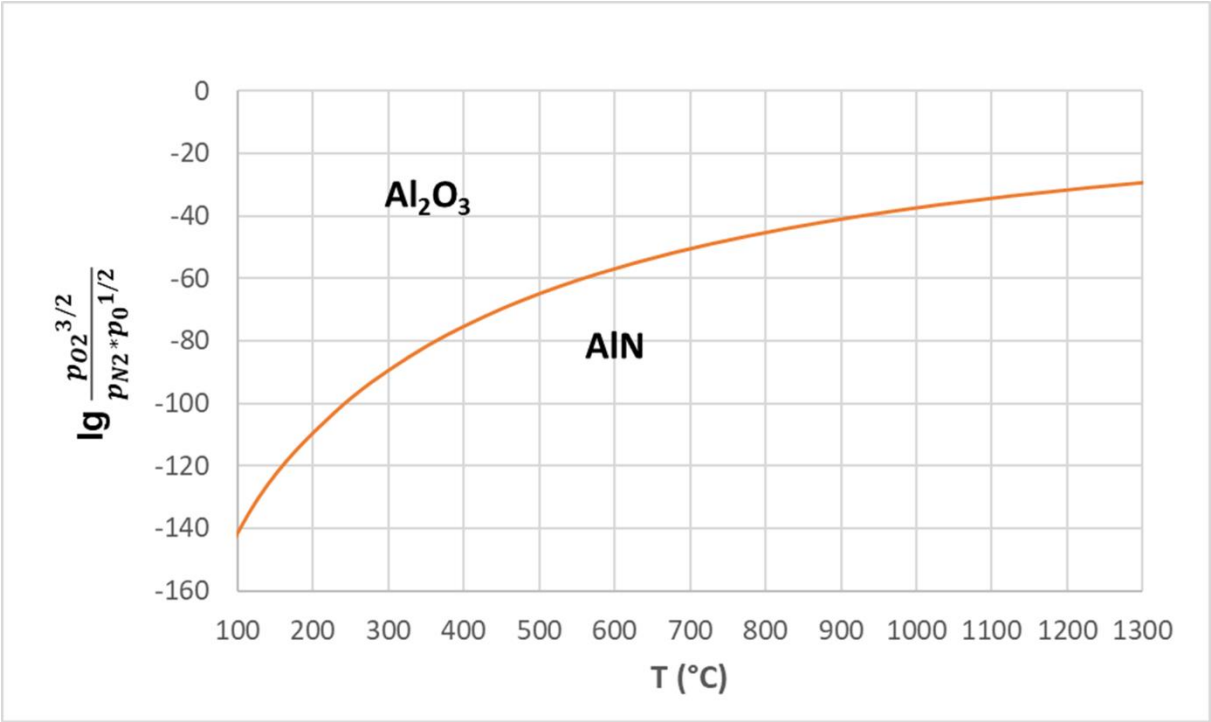

Fig. 15 Stability diagram of AlN and Al_2O_3 phases (according to $2AlN + 1.5O_2 = Al_2O_3 + N_2$) as function of temperature and partial pressures (calculated from the data of [39])

Now, let us discuss the large endothermic peak in Fig.14, which is divided into two parts: into the first part below the macroscopic melting point of Cu (10.9 J/g * 0.153 g = 1.67 J) and into the second part above the same (27.4 J/g * 0.153 g = 4.19 J).

As follows from Fig.14, the onset temperature of this large endothermic peak is 954 °C. However, it is lower than the temperature at which the surface oxide on Cu crystals will dissociate (= 975 °C, see Fig. 9, the cross section of line between the Cu_2O/Cu(s) line and the horizontal „p1" lines) and it is also lower than the temperature at which the sublimation of Cu starts (= 1,010 °C, see Fig.9, the intercept of the Cu(s)/Cu(g) line with the horizontal „p1" lines). Therefore, the endothermic process in the T-interval between 954 … 975 °C (i.e. the first small endothermic peak in Fig.14) is much probably due to the melting of Cu nano-layers due to the melting point depression (MPD) of Cu [16]. The melting enthalpy of copper is 9.68 kJ/mol [39]. If this value is multiplied by the Cu-content still in the NML (= 1.79×10^{-5} mol * 0.25 / 0.75 = 5.97 * 10^{-6} mol), the endothermic heat of 0.058 J is obtained.

The second endothermic process takes place at and somewhat above 975 °C, when the surface oxide layer on Cu dissociates (see also Fig. 9). As the exothermic heat of Cu oxidation was found above as about -0.1 J, now its reverse value is found as about +0.1 J due to dissociation of Cu_2O.

The two first processes (premelting of Cu and dissociation of Cu_2O) are responsible for only about 0.058 + 0.1 = 0.158 J, which is only a small fraction (2.7 %) of the total endothermic heat found in Fig.14 (1.67 + 4.19 = 5.86 J). Note that the reverse reaction $Al_2O_3 + N_2 = 2AlN + 1.5O_2$ will not take place (see Fig.15). The rest of the heat is taken by sublimation (at a higher temperature by melting / evaporation) of Cu (see Fig. 9). The sublimation heat of Cu in the T-interval of the first half of the endothermic peak in Fig.14 is around +330 kJ/mol [39]. Multiplying this value by the amount of Cu on the top of the NML ($1.79*10^{-5}$ mol) provides the endothermic heat of about 5.91 J covers the rest of the endothermic heat measured in Fig.14: 5.86 – 0.158 = 5.70 J.

4. Conclusions

In this paper the deposition of Cu/AlN-Al_2O_3 nano-multilayer (6.4 nm Cu divided by 4.2 nm AlN-Al_2O_3, repated 200 times, covered on both sides by AlN-Al_2O_3) on steel substrate is reported by magnetron sputtering method. Complex structural and thermal behaviour of the NML was found as follows.

Starting from about 400 °C extensive coarsening of Cu nanocrystallites within the multilayer was observed by XRD, which can be related to the migration of copper, reasonably via the mechanism of solid-state diffusion, as a consequence of the poor wetting of AlN-Al_2O_3 layer by liquid copper (also measured here). Part of the initial Cu even formed micron-sized reservoirs within the NML, while the formation of Cu whiskers was also observed from 350 °C on the top surface of the NML. Due to increased temperature and to the different heat expansion coefficients of Cu and the AlN-Al_2O_3 diffusion barriers the latter cracked and Cu appeared on the top surface of the NML from the temperature of 250 °C. Below about 900 °C it probably took place as a solid state flow, leading to faceted copper micro-crystals. However, above about 900 °C one possible explanation to the observed faceted – rounded transformation of the Cu crystals is the pre-melting of Cu, which might took place due to its high specific surface area in the NML. However, the roundening process can also take place via solid state diffusion where the driving force is the reduction of the specific surface area of the Cu crystals.

In addition to that, secondary processes also took place. It was the surface oxidation of the copper crystals at the top of the NML and the partial oxidation of AlN, both due to residual oxygen in the vacuum chamber at around 500 … 800 °C (both are exothermic processes). Above 975 °C dissociation of Cu_2O took place on the surface of copper crystals, while above 1,010 °C sublimation of copper took place (both being endothermic processes).

It can be concluded, that the obtained results offer promising opportunities and routes for advanced low-temperature joining applications. Even if the Cu crystals appear on the top surface of NML via solid flow without pre-melting (which takes place only above 900 °C), these Cu crystals can provide joining at 250 °C (especially above 450 °C), if two such NML-s are prepared on two steel substrates and if they are turned to each other face-to-face.

Acknowledgments

This study was carried out as part of the GINOP-2.3.2-15-2016-00027 "Sustainable operation of the workshop of excellence for the research and development of crystalline and amorphous nanostructured materials" project implemented in the framework of the Szechenyi 2020 program. The realization of this project was supported by the European Union.

The research work of M. Czagány was supported by the ÚNKP-19-3 New National Excellence Program of the Ministry for Innovation and Technology. The authors are grateful to Mr. Gábor Karacs for the TEM measurement. Courtesy to Innovacios Laboratorium Ltd., (Miskolc, Hungary) for support of Field Emission Scanning Electron Microscope (SEM) Hitachi S-4800 equipped with Bruker AXS Energy-dispersive X-ray Spectrometer (EDS) system.

Conflict of Interest

The authors declare that they have no conflict of interest.

References

1. Zhou Y (2008) Microjoining and Nanojoining - 1st Edition. Woodhead Publishing
2. Janczak-Rusch J, Kaptay G, Jeurgens LPH (2014) Interfacial Design for Joining Technologies: An Historical Perspective. J Mater Eng Perform 23:1608–1613. https://doi.org/10.1007/s11665-014-0928-5
3. Zou C, Gao Y, Yang B, Zhai Q (2010) Synthesis and DSC study on Sn3.5Ag alloy nanoparticles used for lower melting temperature solder. J Mater Sci Mater Electron 21:868–874. https://doi.org/10.1007/s10854-009-0009-y
4. Wang Y, Liu W, Liu W, et al (2017) Synthesis of SnAgCu nanoparticles with low melting point by the chemical reduction method. Microelectron Reliab 78:17–24. https://doi.org/10.1016/j.microrel.2017.07.069
5. Azqadan E, Ekrami A (2017) Transient liquid phase bonding of dual phase steels using Fe-based, Ni-based, and pure Cu interlayers. J Manuf Process 30:106–115. https://doi.org/10.1016/j.jmapro.2017.09.006

6. Eustathopoulos N, Voytovych R (2016) The role of reactivity in wetting by liquid metals: a review. J Mater Sci 51:425–437. https://doi.org/10.1007/s10853-015-9331-3
7. Kaptay G (2008) A unified model for the cohesive enthalpy, critical temperature, surface tension and volume thermal expansion coefficient of liquid metals of bcc, fcc and hcp crystals. Mater Sci Eng A 495:19–26. https://doi.org/10.1016/j.msea.2007.10.112
8. Kaptay G (2020) A coherent set of model equations for various surface and interface energies in systems with liquid and solid metals and alloys. Adv Colloid Interface Sci 283:102212. https://doi.org/10.1016/j.cis.2020.102212
9. de Prado J, Sánchez M, Ruiz A, Ureña A (2020) Effect of brazing temperature, filler thickness and post brazing heat treatment on the microstructure and mechanical properties of W-Eurofer joints brazed with Cu interlayers. J Nucl Mater 533:152117. https://doi.org/10.1016/j.jnucmat.2020.152117
10. Benedetti A, Gambaro S, Valenza F, et al (2018) Ag and AgCu as brazing materials for Ti6Al4V-Y3Al5O12 joints: Does ennoblement affect the galvanic behaviour in seawater? Electrochim Acta 283:155–166. https://doi.org/10.1016/j.electacta.2018.06.084
11. Chen ZB, Bian H, Hu SP, et al (2018) Surface modification on wetting and vacuum brazing behavior of graphite using AgCu filler metal. Surf Coatings Technol 348:104–110. https://doi.org/10.1016/j.surfcoat.2018.05.039
12. Schwartz MM (2003) Brazing, Second Edi. ASM International, Ohio, USA
13. Pigozzi G, Antušek A, Janczak-Rusch J, et al (2012) Phase constitution and interface structure of nano-sized Ag-Cu/AlN multilayers: Experiment and ab initio modeling. Appl Phys Lett 101:181602. https://doi.org/10.1063/1.4761471
14. Mei QS, Lu K (2007) Melting and superheating of crystalline solids: From bulk to nanocrystals. Prog Mater Sci 52:1175–1262. https://doi.org/10.1016/j.pmatsci.2007.01.001
15. Wang Z, Jeurgens LPH, Sigle W, Mittemeijer EJ (2015) Observation and Origin of Extraordinary Atomic Mobility at Metal-Semiconductor Interfaces at Low Temperatures. Phys Rev Lett 115:016102. https://doi.org/10.1103/PhysRevLett.115.016102
16. Kaptay G, Janczak-Rusch J, Jeurgens LPH (2016) Melting Point Depression and Fast Diffusion in Nanostructured Brazing Fillers Confined Between Barrier Nanolayers. J Mater Eng Perform 25:3275–3284. https://doi.org/10.1007/s11665-016-2123-3

17. Vegh A, Kaptay G (2018) Modelling surface melting of macro-crystals and melting of nano-crystals for the case of perfectly wetting liquids in one-component systems using lead as an example. Calphad 63:37–50. https://doi.org/10.1016/j.calphad.2018.08.007
18. Kaptay G (2018) The chemical (not mechanical) paradigm of thermodynamics of colloid and interface science. Adv Colloid Interface Sci 256:163–192. https://doi.org/10.1016/j.cis.2018.04.007
19. Adams DP (2015) Reactive multilayers fabricated by vapor deposition: A critical review. Thin Solid Films 576:98–128. https://doi.org/10.1016/j.tsf.2014.09.042
20. Simões S, Viana F, Koçak M, et al (2011) Diffusion bonding of TiAl using reactive Ni/Al nanolayers and Ti and Ni foils. Mater Chem Phys 128:202–207. https://doi.org/10.1016/j.matchemphys.2011.02.059
21. Yi J, Zhang Y, Wang X, et al (2016) Characterization of Al/Ti Nano Multilayer as a Jointing Material at the Interface between Cu and Al2O3. Mater Trans 57:1494–1497. https://doi.org/10.2320/matertrans.M2016126
22. Liu Y, Lin S, Zhang H, et al (2020) Reactive wafer bonding with nanoscale Ag/Cu multilayers. Scr Mater 184:1–5. https://doi.org/10.1016/j.scriptamat.2020.03.043
23. Janczak-Rusch J, Wojarski L, Lehmert B, et al (2012) Deposition and Utilization of Nano-Multilayered Brazing Filler Systems Designed for Melting Point Depression Micro-and Nanojoining View project Dissertation: Bedarfsgerechtes Spritzen WC-basierter HVOF-Cermet-Schichten View project Deposition and utilizat
24. Kaptay G, Janczak-Rusch J, Pigozzi G, Jeurgens LPH (2014) Theoretical Analysis of Melting Point Depression of Pure Metals in Different Initial Configurations. J Mater Eng Perform 23:1600–1607. https://doi.org/10.1007/s11665-014-0885-z
25. Cancellieri C, Klyatskina E, Chiodi M, et al (2018) The Effect of Interfacial Ge and RF-Bias on the Microstructure and Stress Evolution upon Annealing of Ag/AlN Multilayers. Appl Sci 8:2403. https://doi.org/10.3390/app8122403
26. Araullo-Peters V, Cancellieri C, Chiodi M, et al (2019) Tailoring Fast Directional Mass Transport of Nano-Confined Ag–Cu Alloys upon Heating: Effect of the AlN Barrier Thickness. ACS Appl Mater Interfaces 11:6605–6614. https://doi.org/10.1021/acsami.8b19091
27. Lehmert B, Janczak-Rusch J, Pigozzi G, et al (2015) Copper-Based Nanostructured Coatings for Low-Temperature Brazing Applications. Mater Trans 56:1015–1018. https://doi.org/10.2320/matertrans.MI201419
28. Frank Moszner, Claudia Cancellieri, Christoph Becker, et al (2016) Nano-Structured

Cu/W Brazing Fillers for Advanced Joining Applications. J Mater Sci Eng B 6:. https://doi.org/10.17265/2161-6221/2016.9-10.003

29. Moszner F, Cancellieri C, Chiodi M, et al (2016) Thermal stability of Cu/W nano-multilayers. Acta Mater 107:345–353. https://doi.org/10.1016/j.actamat.2016.02.003
30. Cancellieri C, Moszner F, Chiodi M, et al (2016) The effect of thermal treatment on the stress state and evolving microstructure of Cu/W nano-multilayers. J Appl Phys 120:195107. https://doi.org/10.1063/1.4967992
31. European Steel and Alloy Grades/Numbers. http://steelnumber.com. Accessed 24 Sep 2020
32. Druzhinin AV, Ariosa D, Siol S, et al (2019) Effect of the individual layer thickness on the transformation of Cu/W nano-multilayers into nanocomposites. Materialia 7:100400. https://doi.org/10.1016/j.mtla.2019.100400
33. Falsafein M, Ashrafizadeh F, Kheirandish A (2018) Influence of thickness on adhesion of nanostructured multilayer CrN/CrAlN coatings to stainless steel substrate. Surfaces and Interfaces 13:178–185. https://doi.org/10.1016/j.surfin.2018.09.009
34. Çomakli O (2020) Influence of CrN, TiAlN monolayers and TiAlN/CrN multilayer ceramic films on structural, mechanical and tribological behavior of β-type Ti45Nb alloys. Ceram Int 46:8185–8191. https://doi.org/10.1016/j.ceramint.2019.12.046
35. Monclús MA, Karlik M, Callisti M, et al (2014) Microstructure and mechanical properties of physical vapor deposited Cu/W nanoscale multilayers: Influence of layer thickness and temperature. Thin Solid Films 571:275–282. https://doi.org/10.1016/j.tsf.2014.05.044
36. Janczak-Rusch J, Chiodi M, Cancellieri C, et al (2015) Structural evolution of Ag–Cu nano-alloys confined between AlN nano-layers upon fast heating. Phys Chem Chem Phys 17:28228–28238. https://doi.org/10.1039/C5CP00782H
37. Clemens BM, Gay JG (1987) Effect of layer-thickness fluctuations on superlattice diffraction. Phys Rev B 35:9337–9340. https://doi.org/10.1103/PhysRevB.35.9337
38. Schweitz KO, Rätzke K, Foord D, et al (2000) The microstructural development of Ag/Ni multilayers during annealing. Philos Mag A 80:1867–1877. https://doi.org/10.1080/01418610008219090
39. Barin I (1993) Thermochemical Data of Pure Substances, Second edi. VCh, Weinheim
40. Frisk K (1991) A thermodynamic evaluation of the Cr-N, Fe-N, Mo-N and Cr-Mo-N systems. Calphad 15:79–106. https://doi.org/10.1016/0364-5916(91)90028-I
41. RHEE SK (1971) Wetting of Ceramics by Liquid Metals. J Am Ceram Soc 54:332–

334. https://doi.org/10.1111/j.1151-2916.1971.tb12307.x
42. Ownby PD, Liu J (1988) Surface energy of liquid copper and single-crystal sapphire and the wetting behavior of copper on sapphire. J Adhes Sci Technol 2:255–269. https://doi.org/10.1163/156856188X00264
43. Emsley J (1989) The Elements. Clarendon Press, Oxford
44. Samsonov G (1978) Physico-chemical properties of oxides (in Russian). Moskva Metallurgiia
45. Samsonov G, Vinickii I (1976) Refractory compounds (in Russian). Moskva Metallurgiia
46. Auciello O, Chevacharoenkul S, Ameen MS, Duarte J (1991) Controlled ion beam sputter deposition of W/Cu/W layered films for microelectronic applications. J Vac Sci Technol A Vacuum, Surfaces, Film 9:625–631. https://doi.org/10.1116/1.577377
47. Ábrahám G (1998) Optics. In: Optics. McGraw-Hill, Budapest
48. Levai G, Godzsák M, Török TI, et al (2016) Designing the Color of Hot-Dip Galvanized Steel Sheet Through Destructive Light Interference Using a Zn-Ti Liquid Metallic Bath. Metall Mater Trans A 47:3580–3596. https://doi.org/10.1007/s11661-016-3545-0
49. Kaptay G, Báder E, Bolyán L (2000) Interfacial Forces and Energies Relevant to Production of Metal Matrix Composites. Mater Sci Forum 329–330:151–156. https://doi.org/10.4028/www.scientific.net/MSF.329-330.151
50. Chen H, Lee HY, Ku CS, Wu AT (2016) Evolution of residual stress and qualitative analysis of Sn whiskers with various microstructures. J Mater Sci 51:3600–3606. https://doi.org/10.1007/s10853-015-9680-y
51. Illés B, Krammer O, Hurtony T, et al (2020) Kinetics of Sn whisker growth from Sn thin-films on Cu substrate. J Mater Sci Mater Electron. https://doi.org/10.1007/s10854-020-04180-2
52. Sycheva A, Radanyi A, Gácsi Z (2014) Studying Pressure Induced Whiskers Formation from Sn-Rich Surfaces. Mater Sci Forum 790–791:271–276. https://doi.org/10.4028/www.scientific.net/MSF.790-791.271
53. Dutta I, Burkhard M, Kuwano S, et al (2010) Correlation between surface whisker growth and interfacial precipitation in aluminum thin films on silicon substrates. J Mater Sci 45:3367–3374. https://doi.org/10.1007/s10853-010-4359-x
54. Chen S, Lin J-Y, Hsu C, et al (2013) Ag Whisker Formation in Ag-In-Se Alloys. Metall Mater Trans A 44:5281–5283. https://doi.org/10.1007/s11661-013-2030-2

55. Horváth B, Illés B, Shinohara T, Harsányi G (2013) Copper-oxide whisker growth on tin–copper alloy coatings caused by the corrosion of Cu6Sn5 intermetallics. J Mater Sci 48:8052–8059. https://doi.org/10.1007/s10853-013-7619-8
56. Ohnuma M, Hono K, Linderoth S, et al (2000) Small-angle neutron scattering and differential scanning calorimetry studies on the copper clustering stage of Fe–Si–B–Nb–Cu nanocrystalline alloys. Acta Mater 48:4783–4790. https://doi.org/10.1016/S1359-6454(00)00277-9
57. Yakymovych A, Kaptay G, Roshanghias A, et al (2016) Enthalpy Effect of Adding Cobalt to Liquid Sn-3.8Ag-0.7Cu Lead-Free Solder Alloy: Difference between Bulk and Nanosized Cobalt. J Phys Chem C 120:1881–1890. https://doi.org/10.1021/acs.jpcc.5b09445
58. Kaptay G (2015) Approximated equations for molar volumes of pure solid fcc metals and their liquids from zero Kelvin to above their melting points at standard pressure. J Mater Sci 50:678–687. https://doi.org/10.1007/s10853-014-8627-z
59. Kosolapova T (1986) Properties, synthesis and application of refractory compounds (in Russian). Moskva Metallurgiia